Infrared Physics & Technology 71 (2015) 163–170

Contents lists available at ScienceDirect

Infrared Physics & Technology

journal homepage: www.elsevier.com/locate/infrared

Internal and external stray radiation suppression for LWIR catadioptric telescope using non-sequential ray tracing

Yang Zhu [a,b,*], Xin Zhang [a], Tao Liu [a], Yanxiong Wu [a], Guangwei Shi [a], Lingjie Wang [a]

[a] Key Laboratory of Optical System Advanced Manufacturing Technology, Changchun Institute of Optics, Fine Mechanics and Physics, Chinese Academy of Sciences, Changchun 130033, China
[b] University of Chinese Academy of Sciences, Beijing 100049, China

HIGHLIGHTS

- A compact and re-imaging LWIR catadioptric telescope is designed.
- Internal and external stray radiation is analyzed using non-sequential ray tracing method.
- Infrared material selection is applied to reduce self-emitting stray radiation.
- The mechanical structures are designed to further suppress self-emitting stray radiation.

ARTICLE INFO

Article history:
Received 22 January 2015
Available online 26 March 2015

Keywords:
Stray radiation suppression
Optical design
Optical material selection
Non-sequential ray tracing

ABSTRACT

A long wave infrared imaging system operated for space exploration of faint target is highly sensitive to stray radiation. We present an integrative suppression process of internal and external stray radiation. A compact and re-imaging LWIR catadioptric telescope is designed as practical example and internal and external stray radiation is analyzed for this telescope. The detector is cryogenically cooled with 100% cold shield efficiency of Lyot stop. A non-sequential ray tracing technique is applied to investigate how the stray radiation propagates inside optical system. The simulation and optimization during initial design stage are proceeded to avoid subversive defect that the stray radiation disturbs the target single. The quantitative analysis of stray radiation irradiance emitted by lenses and structures inside is presented in detail. The optical elements, which operate at room-temperature due to the limitation of weight and size, turn to be the significant stray radiation sources. We propose a method combined infrared material selection and optical form optimization to reduce the internal stray radiation of lens. We design and optimize mechanical structures to achieve a further attenuation of internal stray radiation power. The point source transmittance (PST) is calculated to assess the external radiation which comes from the source out of view field. The ghost of bright target due to residual reflection of optical coatings is simulated. The results show that the performance of stray radiation suppression is dramatically improved by iterative optimization and modification of optomechanical configurations.

1. Introduction

Stray radiation is the undesired radiation that can reduce image contrast and infrared system detectivity without sufficient rejection. Stray radiation includes self thermal emission from the optical system, solar radiation out of field and ghost of target [1–5]. Suppression of stray radiation is an interdisciplinary research including optical design, optical material, mechanical structure design, fabrication technique, surface scattering and image analysis. With the increasing requirement for accuracy of faint target detection, the suppression level dominates the performance of infrared system. We should devote ourselves to the investigation of both internal and external stray radiation.

The LWIR band (8–11 μm) is chosen because it presents a window in transmission of optical system and a high sensitivity for detector [6]. The instrument operated in LWIR band places profoundly different considerations of optomechanical design [7]. All substances above absolute zero continuously emit radiation which is proportional to the temperature of substances [8]. The sun

* Corresponding author at: Key Laboratory of Optical System Advanced Manufacturing Technology, Changchun Institute of Optics, Fine Mechanics and Physics, Chinese Academy of Sciences, Changchun 130033, China. Tel.: +86 13214461089.
E-mail address: zhuyang_1989@126.com (Y. Zhu).

http://dx.doi.org/10.1016/j.infrared.2015.03.008
1350-4495/

emission almost contains all the waveband. For cooled surfaces, the self-emission in infrared waveband accounts for most of the total emission. The sun emission out of LWIR band is blocked by filter and cannot be responded by detector. The temperature of the shields and baffles due to the sun emission of other waveband is controlled to be less than 293 K. A major contribution to stray radiation in LWIR band is the thermal emission from the telescope itself and increases rapidly with temperature [9]. The higher absorption of baffles and housings coated with black paints is benefit to external stray radiation rejection, but may increase internal stray radiation seriously. Thus integrative suppression of internal and external stray radiation in LWIR band is needed. The optical configuration and lens material selection to reduce stray radiation should also be considered during the preliminary conceptual design stage. A lot of previous investigations have proved that the non-sequential ray tracing is a powerful technology to achieve reflecting, absorbing and scattering of opto-mechanical surface with graphical representation. Monte Carlo method based on probabilistic ray tracing can also be performed in which the surface scattering properties are modeled by a probabilistic function rather than Snell's law [10–13].

This article presents a typical catadioptric infrared telescope as an example for agile spacecraft mission. The optical elements and mechanical structures, which operate at room-temperature without any refrigeration, are applied to reduce the weight and cost of system, improve the reliability and operation life and also makes harder for internal stray radiation rejection. The dewar and detector with 256 × 256 pixels operate under cryogenic temperature of 77 K. The paper is organized as follows: in Section 2, the methods of integrative stray radiation analysis and calculation of refractive lens emissivity are described. In Section 3, a comparative investigation of lens design and self stray radiation between different infrared material compositions is given and discussed. In Section 4, the structures are designed and optimized to further suppress the self-emitting stray radiation of optics. The integrative suppression of internal and external stray radiation is presented. In Section 5, the ghost image simulation due to residual reflection of multilayer films is stated. In Section 6, the performance of stray radiation suppression is discussed and assessed by a visualization of stray radiation distribution.

2. Stray radiation analysis process

The general process for stray radiation suppression of infrared system, explaining the evolution of optomechanical design and modification, is shown in Fig. 1 and expatiated as follows. For each analysis loop, (1) identify parameters of optical system including focal length, entrance pupil diameter, waveband, field of view (FOV) and environment temperature. (2) Specify stray radiation budget according to SNR requirement. (3) Determine general optical design form and lens materials to reduce internal stray radiation of warm optical surfaces. (4) Design and optimize baffles and mechanical housings to reduce external stray radiation. (5) Build optomechanical model and input surface parameters for analysis. (6) Perform analysis of external and internal stray radiation. (7) Compare the results with stray radiation budget. If results do not meet the requirements, optimize and modify optomechanical model by another loop. (8) Obtain the final optomechanical parameters. Due to the limit of article length, part of the analysis process is not presented.

2.1. Radiant irradiance calculation

The element with self-emission is regarded as greybody in infrared system. The radiant exitance M of greybody is given by [8].

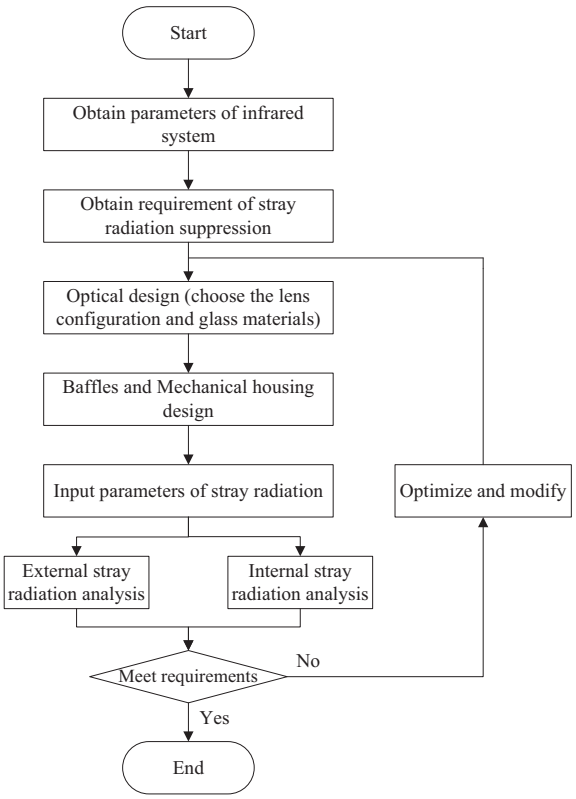

Fig. 1. Overall flowchart of integrative suppression and optimization for stray radiation.

$$M(\lambda,T)=\frac{\varepsilon(\lambda,T)}{\lambda^5}\frac{c_1}{[e^{c_2/\lambda T}-1]} \tag{1}$$

where ε is surface emissivity of greybody, T is temperature of surface. The constants are equal to $c_1 = 2\pi hc^2 = 3.7418 \times 10^{-16}$ W m^2 and $c_2 = hc/k = 1.4388 \times 10^{-2}$ m K, where h is Plank's constant and k is Boltzmann constant. The radiant flux of greybody is given by

$$\Phi=\int_S\int_\lambda M(\lambda,T)d\lambda ds=\int_S\int_\lambda\frac{\varepsilon(\lambda,T)}{\lambda^5}\frac{c_1}{[e^{c_2/\lambda T}-1]}d\lambda ds \tag{2}$$

where S is area of emitting surface, λ is radiant wavelength band. Eq. (2) states that the radiant flux of surface is influenced by its emissivity, temperature, area and radiant waveband. The radiant waveband is determined by target, detector and atmosphere window ahead of the system and is hard to be modified. For practical engineering application of stray radiation analysis, we prefer proper optomechanical forms and materials to reduce the amount, emissivity and area of optical surfaces. We can also optimize the emissivity of diffuse black mechanical surfaces to balance the influences between external and internal stray radiation.

2.2. Emissivity of surface

For extended target, the energy loss is related to the transmission of optical system and the intervening medium [14]. The energy loss introduced by surface mostly is residual reflection but not absorption. The contribution to the lens emissivity is the absorption of intervening infrared material. According to Kirchhoff's Law, the absorption α and optical element emissivity ε are equal for a material in thermal equilibrium [15]. For optical lens, the emissivity be expressed as [16]

$$\varepsilon = 1 - e^{-Az} \approx Az \tag{3}$$

where z is propagation distance within optical material, A is absorption coefficient (cm^{-1}) at the experimental temperature and given wavelength, and mostly the absorption coefficient data is offered by material producers at 298 K and 10.6 μm. As the value of Az is small enough, the emissivity ε can be approximately equal to Az.

Typical characteristics of several representative materials used for LWIR are given in Table 1 to determine appropriate material selection for improving performance of image quality and stray radiation suppression [17–23]. We often use high refraction index materials to reduce aberration. From Table 1, Zinc sulfide (ZnS) can be seen to have the worst stray radiation performance of all the materials listed, and need to be considered and applied carefully. Zinc selenium (ZnSe) and GASIR1 offer a better stray radiation property comparing with germanium (Ge) and ZnS. Fabricating GaAs creates toxins and would only be used in special fields. The new compositions of chalcogenide materials are still under investigation.

3. Lens design and self radiation calculation of optical elements

For large entrance pupil and long focal length cooled system, the cost, size and weight of purely dioptric system increase dramatically. We should make careful considerations on optical configuration beforehand to achieve all requirements [24]. We prefer re-imaging catadioptric system with Cassegrain-like type front end and a refractive relay group to achieve better image quality, fewer warm surfaces, lower stray radiation and shorter overall length. The re-imaging type with field stop and Lyot stop can suppress internal and external stray radiation effectively. The refractive relay group can balance the non-paraxial aberrations coma and astigmatism introduced by mirrors and improve the field of view. We speed up F number of primary mirror properly, so that the stray radiation suppression can benefit from the reduction of field stop aperture. We choose a plane secondary mirror instead of aspherical convexity to reduce the cost and difficulty of fabrication.

Two typically design examples of same specifications are given to compare the self stray radiation power caused by different lens materials and relay group forms. The first order parameters of LWIR system are presented as example in Table 2. In the waveband 8–11 μm, two examples are designed and optimized to achieve diffraction-limited by Code V, and the stray radiation are analyzed by Lighttools (software from Optical Research Associates, Pasadena, California). The program Code V and Lighttools can be linked together to accomplish several loops of optimization and analysis. The merit function used to optimize the system is based on the transverse ray aberration and wavefront error variance.

Layout of the first type is shown in Fig 2(a). All the materials of three refractive lenses are germanium. The polychromatic diffraction modulation transfer function (MTF), plotting against the spatial frequency in cycles/mm, is shown in Fig. 2(b). The prescriptions of lens data are given in Table 3. The primary mirror, third and fifth surface are aspheric with 8th orders.

Table 2
First order parameters of LWIR optical system as practical example.

Effective focal length	200 mm
F number	2
Field of view	3° × 3°
Spectral bandwidth	8–11 μm
Pixel size of detector	30 μm × 30 μm
Obstruction radio	<0.35
Environment temperature	293 K
MTF of optics (at Nyquist frequency)	>0.5

The second type, which utilized ZnSe, Ge and ZnSe as the materials of refractive relay group, is shown in Fig 3(a). The polychromatic MTF plot is shown in Fig. 3(b). Table 4 lists the lens data prescription and Table 5 lists the self-emitting stray radiation results. The primary mirror, fourth and eighth surface are aspheric with 8th orders. The overall length is less than 105 mm, and the central obscuration radio is 0.34.

We can get material absorption coefficients from Table 1 and thickness of refractive lens from Table 3.Then we put them into Eq. (3) and obtain the emissivity ε of optical element. After that, we put emissivity, wavelength band and temperature into Eq. (2) to obtain the radiant flux of optical element. The transmissivity of coatings are set 99% for all materials to simplify the calculations. The self-emitting stray radiation contributed by optical surfaces is simulated by Lighttools based on non-sequential ray tracing technique. The number of initial rays is 100 million to get a smoother image on detector and the results are given in Table 5. Compared with the previous one, the material composition of ZnSe, Ge and ZnSe reduces the self stray radiation power by 40.1%. The reason is that germanium has a much larger absorption coefficient and a larger emissivity than ZnSe and introduces more stray radiation. The average MTF of all fields drop from 0.46 to 0.43 because germanium has a much larger refractive index and Abbe Number and is beneficial to the aberration correction and chromatic dispersion control. The radiation contributed by refractive lens is the main part of self-radiation emitted by optics and is difficult to reduce by mechanical structures.

In general, the second optical design configuration is a better choice to simultaneously improve the performance of image quality and stray radiation suppression, and is prepared for the followed internal and external stray radiation analysis.

4. Internal and external stray radiation analysis

To satisfy faint targets detecting in present of a strong source out of field and self-radiation of optomechanical structures, internal and external stray radiation should be analyzed together in particular. Minimizing stray radiation on focal plane is accomplished by several iterative processes of design and analysis as

Table 1
Properties of some LWIR materials.

LWIR material	Refractive index at 10 μm	Effective Abbe number (8–12 μm)	Transmission range (μm)	Absorption coefficient at 298 K and 10.6 μm (cm^{-1})
Ge (monocrystalline)	4.0032	856.1	1.8–17	⩽0.02
Ge (polycrystalline)	4.0032	856.1	1.8–17	0.035
ZnSe	2.4066	57.8	0.5–16	0.0005
ZnS	2.2002	22.9	1–12	0.08
GASIR1	2.4944	119.4	0.8–16	0.007–0.009
GaAs	3.2735	88.4	2–14	0.01
AMTIR1	2.4979	110	0.7–14	0.01

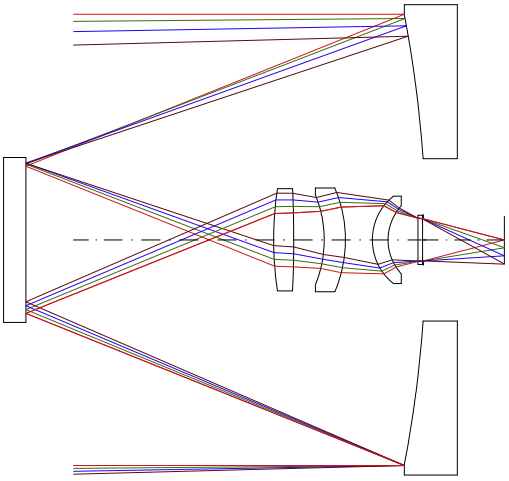

(a) 2D-Layout of Ge -Ge- Ge materials composition

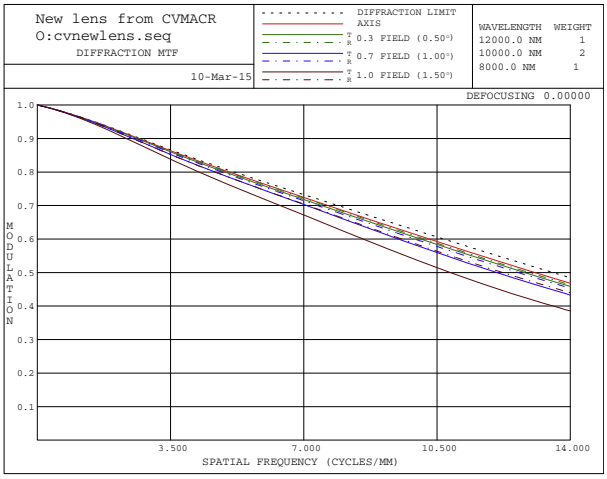

(b) MTF curves of Ge -Ge- Ge materials composition

Fig. 2. (a) 2D-layout of Ge–Ge–Ge materials composition and (b) MTF curves of Ge–Ge–Ge materials composition.

Table 3
Optical design data prescription of Ge–Ge–Ge materials composition.

Surface no.	Type	Radius	Thickness	Glass	Conic
0	Standard	–	∞		
1	Aspherical	−255.46 mm	89.429 mm	MIRROE	−1.7931
2	Standard	∞	55.39	MIRROE	
3	Aspherical	67.223	4.489	Germanium	−2
4	Standard	−445.414	6.807		
5	Aspherical	25.937	4.76	Germanium	1.097
6	Standard	−27.621	6		
7	Standard	12.306	3.513	Germanium	
8	Standard	10.958	6.647		
9	Standard	∞	1	Germanium	
10	Standard	∞	18.165		

presented in Fig. 1. The internal stray radiation is significantly influenced by emissivity, area and emitted solid angle of optomechanical surfaces. Due to the optimization and modify of mechanical structures, the internal stray radiation power of optics further attenuates from 1.03×10^{-5} W to 7.14×10^{-6} W .

4.1. Baffles and mechanical housings design

The main baffle is designed typically to meet the criteria that, for the external stray light out of evadable angle 45°, no first diffuse reflections from the baffle reach the primary mirror. The secondary mirror shade, main baffles and shields need to block the direct ray of stray light and allow the unobscured-imaging rays without vignetting [25]. Thus the external stray radiation can be suppressed by several orders of magnitude. Radiation emitted from critical surfaces directly arrives on detector without any reduction of mechanical structures. All the optical elements and mechanical structures seen by detector directly can be regarded as critical objects. We combine the forward and backward non-sequential ray tracing to find the critical surface. Mostly, the main baffle vans and structures around field stop are critical objects. Secondary hat shading is designed to keep away the stray light near FOV from reaching detector directly. However, the size of secondary hat shading would increase center obstruction and degrade image quality.

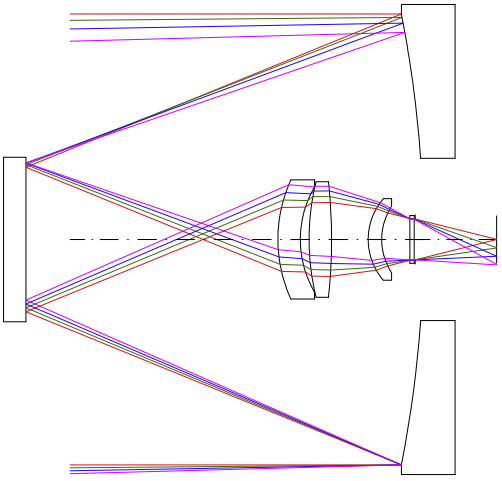

(a) 2D-Layout of ZnSe-Ge- ZnSe Materials composition

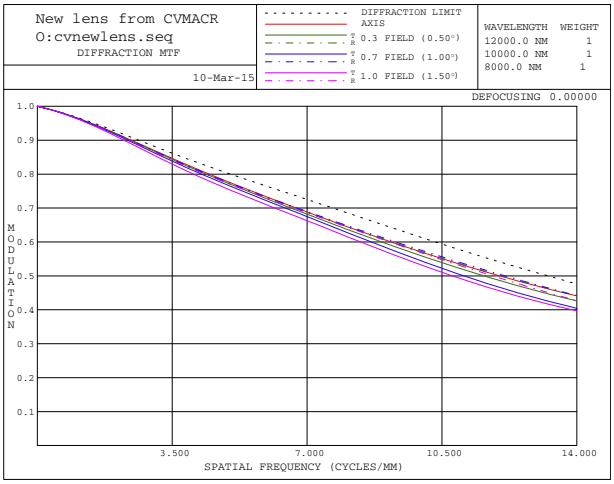

(b) MTF curves of ZnSe-Ge- ZnSe Materials composition

Fig. 3. (a) 2D-layout of ZnSe–Ge–ZnSe materials composition and (b) MTF curves of ZnSe–Ge–ZnSe materials composition.

Table 4
Optical design data prescription of ZnSe–Ge–ZnSe materials composition.

Surface No.	Type	Radius	Thickness	Glass	Conic
0	Standard	–	∞		
1	Aspherical	−252 mm	88.4 mm	MIRROE	−1.929
2	Standard	∞	56.03	MIRROE	
3	Standard	31.607	5	ZnSe	
4	Aspherical	23.706	1.935		1.6
5	Standard	53.822	5	Germanium	
6	Standard	−122.018	8.153		
7	Standard	13.764	3	ZnSe	
8	Aspherical	13.076	6.26		0.325
9	Standard	∞	1	Germanium	
10	Standard	∞	18.1		

The initial and final structures of example system are shown in Fig. 4, including optics, baffles, shades, shields and dewar. Several modifications have been achieved to improve the stray radiation suppression level. The hat shading of secondary mirror is changed into a thin cone and traps are filled in the blanks between the hat shading and mirror. A conical dewar with baffles is designed to reduce stray radiation. A nosecone is placed in the center obstruction part of second mirror and a golden dot with high reflectivity is located in the central of dewar window to further reduce self radiation. Both golden dot and nose cone need to match the obstruction introduced by secondary mirror and hat shading. Due to the suppression with the combination of nose cone and golden dot, the stray radiation power emitted by the front part of field stop is reduced from 2.17×10^{-5} W to 4.24×10^{-7} W and the stray radiation power of the main baffle is reduced from 5.57×10^{-6} W to 2.71×10^{-6} W.

4.2. Internal stray radiation analysis

Though a low-emissivity surface can reduce the amount of self-emitting thermal energy, it also lead to glints and other artifacts that increase the scattered light. The mirrors and lens scatter models are taken from previous published articles [24] and the structures with diffuse black paints are approximately regarded as Lambertain scatter to simplify simulation. The emissivity of components, especially the critical surfaces, need to be optimized and modified carefully.

The number of non-sequential rays is 100 million for each analysis loop. The initial absorption of the structures is 0.8. The absorption of the structures facing to the detector needs to be optimized preferentially. After several integrative optimization loops, we obtain the final emissivity distribution of components and stray radiation power on detector in Table 6. The emissivity of lens 1and lens 3 is a little different due to the different material thicknesses. Compared with Table 5, total optics radiation performance has made further improvement by dropping from 1.03×10^{-5} W to 7.14×10^{-6} W as field stop, Lyot stop, dewar, golden dot, baffles and vanes were designed and optimized. The total thermal power on focal plane is 2.19×10^{-5} W. The percent contributed by optics is 32.6%. Cone of field stop, main baffle and secondary mirror shade distinctly dominated the residual stray radiation power.

Table 5
Comparison of self-emitting radiation from different optical elements.

Objects	Ge–Ge–Ge materials composition	ZnSe–Ge–ZnSe materials composition
Primary mirror	3.04×10^{-6} W	3.17×10^{-6} W
Secondary mirror	3.41×10^{-6}	3.52×10^{-6}
Lens 1	3.53×10^{-6}	8.95×10^{-8}
Lens 2	3.90×10^{-6}	3.50×10^{-6}
Lens 3	3.38×10^{-6}	5.51×10^{-8}
Sum self-emitting stray radiation	1.72×10^{-5}	1.03×10^{-5}

4.3. External stray radiation analysis

Outside the atmosphere, the deep-space background can be equivalent to the 4 K blackbody, and its long wave infrared radiation can be ignored [26]. If the orbit is high enough, the earth-atmosphere radiation can also be ignored. The dominant external stray source out of field is the sun, which can be regarded as 5700 K blackbody in engineering. The solar radiant exitance M_{sun} can be calculated by Eq. (1) in 8–11 μm spectral band. The solar radiant irradiance M'_{sun} in entrance aperture of infrared system can be obtained by

$$M'_{sun} = M_{sun}\left(\frac{R_{sun}}{d_{sun\text{-}optics}}\right)^2 \cos\theta_{sun} \tag{4}$$

where R_{sun} is solar radius, $d_{sun\text{-}optics}$ is distance between sun and optical system, and θ_{sun} is the angle of sunlight and optical axis. When θ_{sun} is zero, M'_{sun} is 1.109×10^{-6} W/mm^2 in entrance aperture.

For this example system, the sun is expected to be at least 45° off-axis. PST is a common method to evaluate the rejection characters of external stray radiation. The PST is defined by

$$\mathrm{PST} = \frac{E_d(\theta)}{E_i(\theta)} \tag{5}$$

where $E_d(\theta)$ is the stray radiation irradiance on detector, and $E_i(\theta)$ is the stray source irradiance at the entrance aperture. Essentially, PST is a transfer function relating the irradiance at the focal plane to that at the entrance aperture due to a distant point source located at some angle to the optical axis.

An integrated model is generated in Lighttools for non-sequential ray tracing. The PST is depicted in Fig. 5 at various off axis angles. In general, the PST curve falls off monotonously with a few sub-peaks and terraces. As the direct stray ray is blocked by field stop and Lyot stop, PST declines precipitously from 1.6° to 3°. The sub-peak of 5° is due to the propagation path stray source – primary mirror – secondary mirror – cone of field stop – secondary mirror – refractive lens – detector. The flat between 20° and 35° is owing to the propagation path stray source – cone of field stop – secondary mirror – refractive lens – detector. The PST is 6.19×10^{-6} and the external stray radiation irradiance on detector is 6.93×10^{-12} W/mm^2 at the critical angle of 45°.

5. Ghost image simulation

Ghost images formed by residual reflection of multilayer films can degrade the image contrast and signal to noise ratio especially for large target dynamic range. A ghost image of bright target can disturb dark target detection [27].

Though Zemax has a non-sequential ray tracing capability, it is difficult and inconvenient for Zemax to build complex mechanical structure models. We prefer stray light analysis software Lighttools using non-sequential ray tracing and Monte Carlo method to achieve higher computational efficiency and present an intuitive relationship between target single and ghost. The key ray path analysis can expound how the stray radiation propagates to detector due to both residual reflection and scattering [28]. We use paraxial ray tracing of Code V program to make a preliminary ghost analysis. We can reduce the simulation data amount of Lighttools by filtering the analysis results of Code V. The Code V program evaluates ghost by semi-diameter of the reflected beam (DISC), delta back focal length (DBFL) and pupil ratio. The smaller value

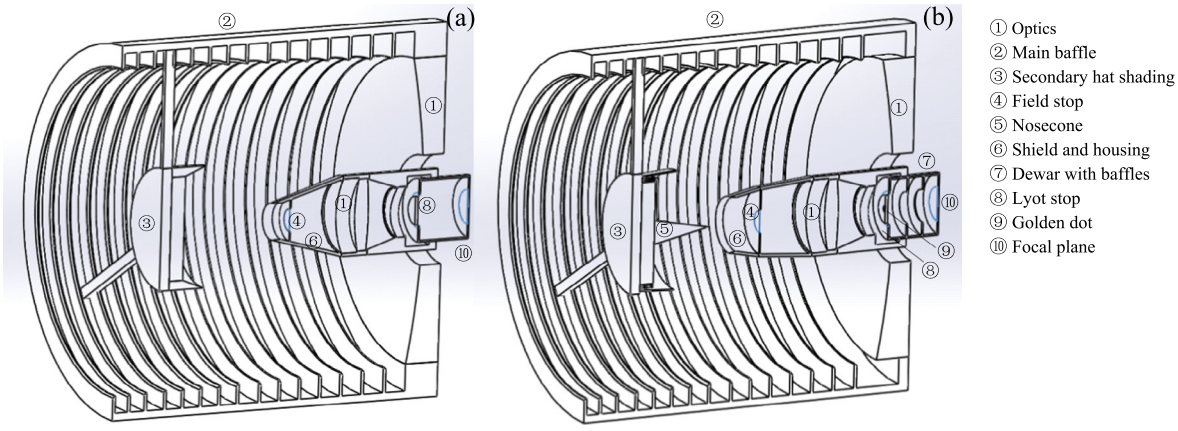

Fig. 4. A comparison between the initial (a) and final (b) optical system structures.

Table 6
Components emissivity and stray radiation power on detector.

Component	Emissivity	Temperature	Stray radiation power
Primary mirror	0.01	293 K	2.28×10^{-6} W
Secondary mirror	0.01	293	2.40×10^{-6}
Lens 1 (ZnSe)	0.00025	293	5.98×10^{-8}
Lens 2 (Ge)	0.00995	293	2.36×10^{-6}
Lens 3 (ZnSe)	0.00015	293	3.65×10^{-8}
Main baffle	0.8	293	2.71×10^{-6}
Secondary mirror shade	0.8	293	2.06×10^{-6}
Nosecone	0.8	293	1.62×10^{-8}
Secondary support rings (facing to primary mirror)	0.1	293	9.15×10^{-7}
Secondary support rings (other surfaces)	0.8	293	1.68×10^{-7}
Rear part of field stop	0.1	293	1.15×10^{-7}
Front part of field stop	0.8	293	4.24×10^{-7}
Cone of field stop (inner)	0.8	293	1.85×10^{-6}
Cone of field stop (outer)	0.8	293	4.32×10^{-6}
Structure between Lens 1 and Lens 2	0.8	293	2.81×10^{-9}
Structure between Lens 2 and Lens 3	0.8	293	4.63×10^{-7}
Structure between Lens 3 and dewar	0.1	293	3.34×10^{-7}
Dewar window (Ge)	0.002	250	1.37×10^{-6}
Dewar baffles	0.8	77	5.54×10^{-8}
Golden dot	0.1	293	3.23×10^{-9}
Total	–	–	2.19×10^{-5}

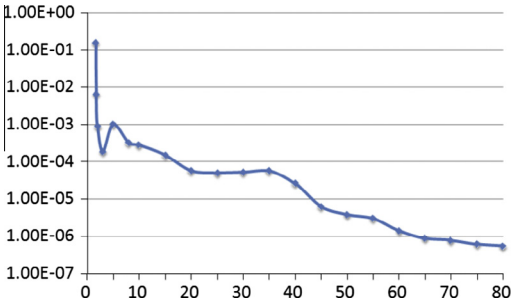

Fig. 5. PST curve of external sources at various incident angles.

of DISC is, the nearer the ghost image is to being in focus. If the DBFL is near zero, the ghost image will be nearly in focus [29]. We write a macro program with the boundary conditions aforementioned to control ghost during optical design and optimization.

Table 7
Ghost image analysis of Code V.

Surface	DBFL	DISC	Pupil ratio
4–3	−9.425087	4.584976	0.892563
6–3	−33.363621	40.231226	4.418946
6–5	−29.259596	58.507105	5.442470
8–7	−15.826389	11.404328	0.262453
8–3	−29.334155	49.973876	4.666054
8–5	−27.251070	56.165925	4.658760
10–3	−45.378494	5.600946	0.792996
10–5	−31.678501	11.711864	1.211723
10–7	−21.949802	16.782309	0.797083
10–9	−0.499616	0.124903	0.971306

The final ghost image analysis of Code V is given partially in Table 7. The ghost image formed by dewar window (Ge) is unavoidable. The DISCs of other ghost images are at least 4.5 mm.

Then the optical model is put into Lighttools for ghost analysis. The incident light power of target at entrance pupil is set to 1 W. The spatial distribution of ghost image on detector is shown in Fig. 6. The irradiance of target image is 88 W/mm^2. The irradiance of ghost speckle besides the target image, which due to the front and rear surface of dewar window, is 3×10^{-3} W/mm^2. The irradiance of ghost annulus formed between the front and rear surface of the first refractive lens is 1.5×10^{-5} W/mm^2. The diffused ghost image is divided into three parts by secondary mirror supporting. The other white parts without any stray radiation are due to the obstruction of secondary mirror.

6. Discussion and assessment of results

To discuss the influence of stray radiation, a numerical simulation is presented in visualization. The irradiance distributions of internal and external stray radiation on detector are showed in Fig. 7. The max irradiance of external stray radiation is 4.02×10^{-10} W/mm^2 when the sun is 45° away from field of view. The max irradiance of internal stray radiation is 5.19×10^{-6} W/mm^2. The stray radiation distributes randomly without obvious flares and spots. Compared with internal and external stray radiation, the influence of ghost is so little that can be ignored.

A planetoid image as original target on focal plane is depicted in Fig. 8(a). A simulation of target with internal and external stray radiation is showed in Fig. 8(b) as comparison. The stray radiation is much lower than the target. The suppression process is successfully performed to prevent stray radiation from disturbing the target detection.

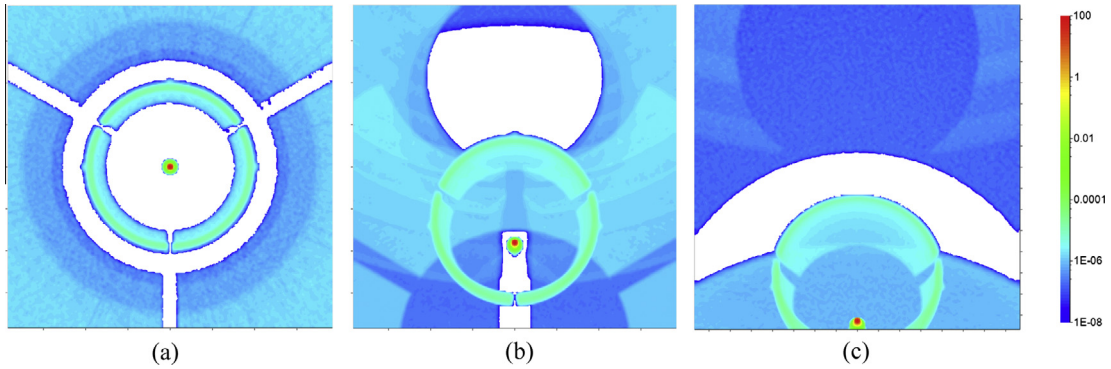

Fig. 6. Spatial distribution of ghost image simulated by non-sequential ray tracing (a) image center, (b) half image height, and (c) image edge (the unit of scale bar is W/mm^2).

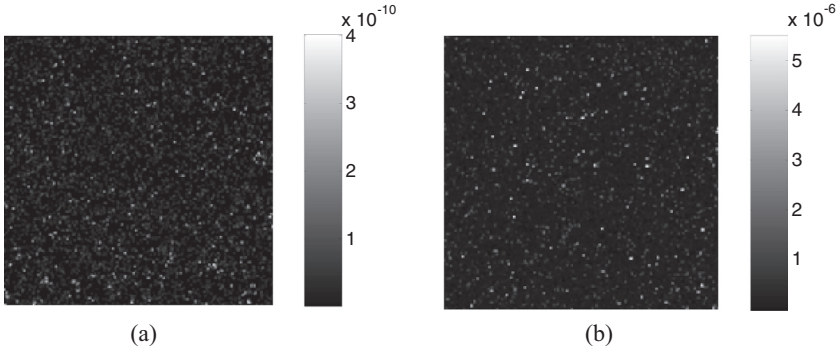

Fig. 7. Irradiance distribution on focal plane (256 × 256 pixels) (a) external stray radiation at 45° and (b) internal stray radiation (the unit of scale bar is W/mm^2).

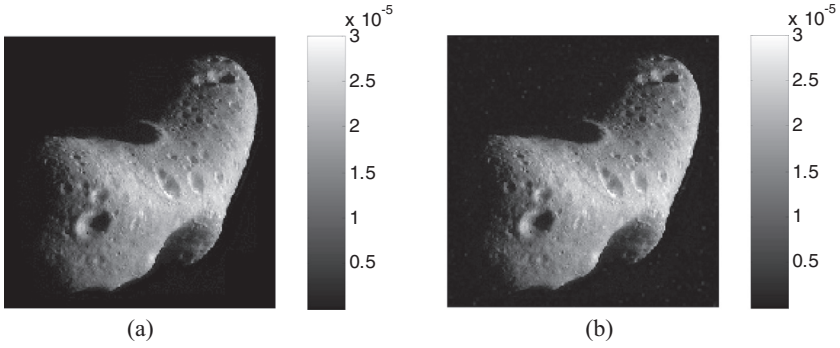

Fig. 8. Numerical simulation (256 × 256 pixels) (a) the original target image and (b) the target image with internal and external stray radiation (the unit of scale bar is W/mm^2).

7. Conclusion

This article described an integrative suppression method of internal and external stray radiation. A cooled LWIR catadioptric optical system was designed and analyzed in detail with different material compositions. We offered a simple method to calculate the emissivity of refractive lens. The refractive material composition of ZnSe–Ge–ZnSe is selected to achieve a much lower self-emitting stray radiation than Ge–Ge–Ge material composition from 1.72×10^{-5} W to 1.03×10^{-5} W. The polychromatic MTF is diffraction-limited. The stray radiation paths can be stored and sifted by non-sequential ray tracing and key ray path analysis. Both external stray radiation and internal radiation were taken into consideration during baffle and housing design stage. The reflection and self-emitting thermal power schedules of structures after optimization were given. The structures including baffle vanes, housing, field stop, Lyot stop, dewar vanes, nosecone and golden dot were optimized to achieve a further attenuation of self-emitting stray radiation of optics from 1.03×10^{-5} W to 7.14×10^{-6} W. The total stray radiation on detector including optics and mechanical structures is 2.19×10^{-5} W. We calculated the PST of external stray radiation at different angles and discussed the reason of curve fluctuation. The ghost image simulation was presented and its influence could be ignored. The final numerical simulation states that the performance of internal and external stray radiation suppression is good enough to avoid the target disturbance.

Conflict of interest

We stated that there is no conflict of interest. We have purchased the genuine software license of Code V and Lighttools and stated the company name in our article. The material data is from several previous papers and website of material companie and have been add in our references.

References

[1] R.P. Breault, Control of stray light,, in: M. Bass (Ed.), Handbook of Optics, vol. 1, McGraw-Hill, 1995 (Chapter 38).
[2] C.R. Boshuizen, M.G. Grimminck, H. Kjeldsen, A.G. Monger, MONS space telescope, part 2: analysis of very high stray-light rejection, Opt. Eng. 47 (2008) 013001.
[3] M.J. Sholl, F.S. Grochocki, J.C. Fleming, R.W. Besuner, P. Jelinsky, M.L. Lampton, Stray light design and analysis of the SNAP telescope, Proc. SPIE 6675 (2007) 66750C.
[4] J.L. Stauder, Stray light design and analysis of the wide-field infrared explorer, Proc. SPIE 3122 (1998) 35–44.
[5] M.M. Talha, Yongtian Wang, Tingcheng Zhang, Design, tolerancing and stray light analyses of a freeform HMD optical system, Optik 121 (2010) 750–755.
[6] M.S. Scholl, Errors in radiance simulation and scene discrimination, Appl. Opt. 21 (10) (1982) 1839–1843.
[7] M.S. Scholl, Design parameters for a two-mirror telescope for stray-light sensitive infrared applications, Infrared Phys. Technol. 37 (1996) 251–257.
[8] R. Siegel, J.R. Howell, Thermal Radiation Heat Transfer, CRC Press, 1992.
[9] M.S. Scholl, Stray light issues for background-limited far-infrared telescope operation, Opt. Eng. 33 (3) (1994) 681–684.
[10] M.N. Akram, Simulation and control of narcissus phenomenon using nonsequential ray tracing. I. Staring camera in 3–5 μm, Appl. Opt. 49 (2010) 964–975.
[11] M.N. Akram, Simulation and control of narcissus phenomenon using nonsequential ray tracing. II. Line-scan camera in 7–11 μm, Appl. Opt. 49 (2010) 1185–1195.
[12] L. Yang, A.X. Qiang, W. Qian, Accurate and fast stray light calculation based on improved backward ray tracing, Appl. Opt. 52 (2013) B1–B9.
[13] A.V. Parvdivtsev, M.N. Akram, Simulation and assessment of stray light effects in infrared cameras using non-sequential ray tracing, Infrared Phys. Technol. 60 (2013) 306–311.
[14] M.S. Scholl, Image-plane incidence for a baffled infrared telescope, Infrared Phys. Technol. 38 (1997) 87–92.
[15] C.M. Conroy, J.D. Guthrie, A.J. Sharkins, B.J. Sparr, R.A. Crocombe, R. Curbelo, An infrared accessory for studying the emissivity of aluminum surfaces, Appl. Spectrosc. 41 (1987) 688–692.
[16] M. Strojnik, Radiometry, in: B. Thompson (Ed.), Handbook of Optical Engineering, Marcel Dekker, 2001, pp. 649–700.
[17] J. Huddleston, A. Symmons, R. Pini, Comparison of the thermal effects on LWIR optical designs utilizing different infrared optical materials, Proc. SPIE 9070 (2014) 90702.
[18] G. Desroches, K. Dalzell, B. Robitaille, Technical considerations for designing low-cost, long-wave infrared objectives, Proc. SPIE 9070 (2014) 907026.
[19] D.C. Harris, Materials for Infrared Windows and Domes: Properties and Performance, SPIE Press, 1999.
[20] CRYSTRAN, zinc selenide, <http://www.crystran.co.uk/usefiles/files/zinc-selenide-znse-data-sheet.pdf>.
[21] CRYSTRAN, zinc sulphide, <http://www.crystran.co.uk/usefiles/files/zinc-sulphide-flir-zns-data-sheet.pdf.
[22] Umicore, Germanium blanks for Infrared Optics, <http://eom.umicore.com/en/infrared-optics/blanks/germanium- data-sheet.pdf>.
[23] DOW Chemical Company, CLEARTRAN data sheet, <http://www.dow.com/products/product/cleartran/>.
[24] P.K. Manhart, K.S. Ellis, J.E. Michalski, Compact, three-mirror anastigmat, with reflective lens, Proc. SPIE 3482 (1998) 282–292.
[25] M.S. Kumar, C.S. Narayanamurthy, A.S. Kiran Kumar, Iterative method of baffle design for modified Ritchey-Chretien telescope, Appl. Opt. 52 (2013) 1240–1247.
[26] Fuyu Huang, Xueju Shen, Gang Li, Guopei Wang, Zhining Zhao, Influence of background radiation on space target detection in the long wave infrared range, Opt. Eng. 51 (2012) 086402.
[27] J.D. Rogers, T.S. Tkaczyk, M.R. Descour, Removal of ghost images by using tilted element optical systems with polynomial surfaces for aberration compensation, Opt. Lett. 31 (2006) 504–506.
[28] Optical research associates, Command reference guide, in: Lighttools Reference Manual, 2010, pp. 329–337.
[29] Optical research associates, Ghost image analysis, in: Code V Reference Manual, 2004, pp. 23–31.